

# Theoretical Determination of Characteristic X-Ray Lines and the Copper $K\alpha$ Spectrum

C. T. Chantler\* and A. C. L. Hayward

*School of Physics, University of Melbourne, Melbourne, Australia*

I. P. Grant

*Mathematical Institute, Oxford University, Oxford, United Kingdom*

(Received 9 May 2009; published 16 September 2009)

Core excitations above the  $K$  edge result in  $K\alpha$  characteristic x-ray emission. Understanding these spectra is crucial for high accuracies in investigations into QED, near-edge x-ray structure and advanced crystallography. We address unresolved quantitative discrepancies between experiment and theory for copper. These discrepancies arise from an incomplete treatment of electronic interactions. By finding solutions to relativistic multiconfigurational Dirac-Fock equations accounting for correlation and exchange corrections, we obtain an accurate reproduction of the peak energies, excellent agreement of theory with experiment for the line shapes, good convergence between gauges, and account for the  $K\alpha$  doublet ratio of  $0.522 \pm 0.003:1$ .

DOI: 10.1103/PhysRevLett.103.123002

PACS numbers: 32.30.Rj, 31.30.jf, 32.80.Hd

Spectroscopic lines resulting from atomic transitions gave the first insights into atomic structure and quantum mechanics [1]. Today, the most well tested theory in nature [2–4], quantum electrodynamics (QED), is probed using the same techniques. The  $K\alpha$  spectrum, a designation from the early days of quantum mechanics, denotes the transition  $2p \rightarrow 1s$ . For heavier atoms, the fine splitting between the  $2p$  states results in distinct peaks for the  $2p_{1/2} \rightarrow 1s$  ( $K\alpha_2$ ) and  $2p_{3/2} \rightarrow 1s$  ( $K\alpha_1$ ) transitions.

These diagram lines (Fig. 1) are the standard candles of x-ray spectroscopy. Wavelength-dispersive experiments, the cornerstone of high accuracies for most of the x-ray regime, are almost exclusively defined by angles, which must be calibrated to these peaks [5]. Alignment of experimental data with physical parameters requires positions and intensities of multiple peaks. Experiments usually have numerous systematics to account for, such as non-linear scaling, diffraction and slit broadening, and the constraint of key parameters yields more critical and definitive results [6,7].

Elementary statistical arguments suggest that the  $K\alpha_2:K\alpha_1$  integrated intensity ratio should be 0.5:1; in reality this ratio increases slowly with atomic number  $Z$  [8–11]. The simplest correct explanation is that the rate of deexcitation of the  $1s$  hole by capture of a  $2p_{1/2}$  electron is greater than that for capture of a  $2p_{3/2}$  electron. Hence by virtue of the faster decay rate, the linewidth of  $K\alpha_2$  is greater than that of  $K\alpha_1$  [12,13]. The increase of the intensity ratio with  $Z$  is supported by nonrelativistic Hartree-Fock calculations [14] especially when shell coupling is taken into account.

Relativistic effects become more pronounced as  $Z$  increases in the transition metal region of the periodic table [15] and fully relativistic theory should be used. Indicators include the growth of intermediate coupling as  $Z$  increases

and the need to introduce energy offsets and dispersion scales [15–17] when trying to reconcile theory and experiment. Most earlier work modeled this by fitting spin-orbit parameters to experimental splittings of diagram lines [15,17]. Other studies indicated the need for relaxation and rearrangement of the atom prior to emission [15,18]. The outermost  $4s$  has usually been ignored [17,19–22].

The complex structure of  $K\alpha$  lines, which are not a simple sharp doublet, has been the source of much speculation: explanations invoke both atomic and solid state mechanisms [14,17]. Generally, the observed spectrum has been fitted to a sum of line profiles whose individual positions and strengths are determined solely by the fitting process without recourse to *ab initio* models. Explanations range from Kondo-like interaction of conduction electrons with core-hole states [23], final-state interactions between the core hole and the  $d$  shell [24], electrostatic interactions of the  $3d$  and  $2p$  shells [25] to  $3l$  shake-up processes [13,19]. The first and last of these explanations have yielded good fits to particular subsets of data.

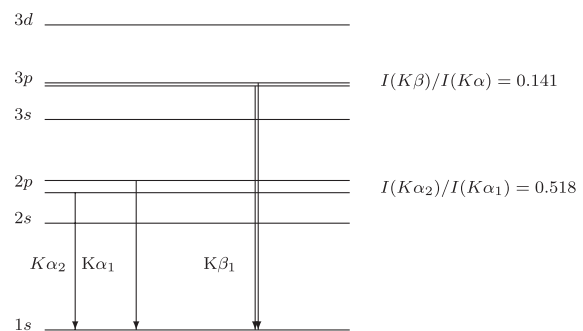


FIG. 1. Dominant radiative transitions between subshells. A statistical population would predict 0.5:1 for  $K\alpha_2/K\alpha_1$ , and 1:6 for  $K\beta/K\alpha$ . Quoted experimental ratios from [8].

Scofield [14] made Dirac-Hartree-Fock (DHF) calculations, and by comparing with earlier work, showed that exchange effects were essential to explain observed intensity ratios throughout the periodic table. Kuhn and Scott [15] made intermediate coupling calculations with Hartree-Fock wave functions suggesting that the most important  $K\alpha$  satellites in the range  $19 \leq Z \leq 32$  were due to an additional vacancy in the  $2p$  subshell. More recently, modelling of  $K\alpha$  spectra has exploited the multi-configurational DHF (MCDHF) computational framework of Grant *et al.* [26–28], often with modifications [8,17,29].

Modern *ab initio* theory for  $N$  electron systems uses atomic state functions (ASFs) which are linear combinations of configuration state functions (CSFs). Each CSF is a sum of antisymmetrized products of atomic orbitals projected onto a subspace of total angular momentum  $J$  and parity  $\pi$  in which the  $N$  electrons are distributed amongst open and closed subshells. The inner electrons of copper,  $Z = 29$ , show strong relativistic effects. Precise measurements of the spectra reveal asymmetric profiles. The importance of copper as a laboratory light source [30] meant that the satellite spectrum was understood empirically at an early stage. The excellent analysis of Deutsch *et al.* [17], using MCDHF calculations to locate the transition energies and amplitudes of the copper  $K\alpha$ , diagram and satellite lines, revealed that the  $3d$  electron hole satellites could indeed account for the observed asymmetry (Fig. 2). These calculations were based on software [28] in which the calculation of transition rates used a common set of orbitals for upper and lower states. This average level model is optimal for neither of the states and limits the accuracy with which energies and transition rates can be predicted. As a starting point for this investigation and with assistance of Deutsch *et al.*, we have reproduced their results.

Fischer and colleagues (Chapter 6, [31]) showed how the multiconfiguration Hartree-Fock procedure (MCHF) can be used for systematic studies of correlation in many-electron atoms. The active space approach focuses atten-

tion on extending the CSF set systematically, starting from a simple atomic configuration, to balance the description of correlation in the ASF. Such independent calculations change the orbitals and the CSF expansion. Calculations of line strengths, etc., based on a common set of orbitals must therefore be modified (Chapter 8, [32]). Olsen *et al.* [33] showed how to use orbital sets from separate calculations to construct a biorthogonal orbital system compatible with MCHF software, enabling striking improvements in predictions of strengths of resonance and intercombination lines in the C III spectrum [34]. These developments have been incorporated in GRASP2K software [35]. The strategies of using the new GRASP2K approach are non-trivial but the intrinsic biorthogonalization permits controlled convergence in difficult problems such as inner-shell hole spectra [36]. To deal with major challenges in core-hole excitation—modelling of convergence and false minima—the best approach is to slowly build up the wave function, beginning with the configuration state only, and adding extra orbitals in steps [32].

Tables I and II show the change in predicted positions of the energies and the transition strengths of the copper  $K\alpha$  diagram lines with the systematic enlargement of the CSF set to include one or more excitations into the subshells, beginning with  $3d^{10}4s^1$ . Earlier MCDHF calculations have achieved agreement with observation to about 2 eV, contrasting with our agreement of 0.01 eV for  $K\alpha_1$  and 0.06 eV for  $K\alpha_2$ . This eliminates the need to introduce additional fitting parameters when deconvolving the observed spectrum. The computational model starts from the matrix of the MCDHF atomic Hamiltonian in the chosen CSF space assuming that the electron-electron interaction is a Coulomb potential. The matrix of the fully retarded relativistic electron-electron interaction is then added and the diagonal matrix elements of the perturbed atomic Hamiltonian are also augmented with QED corrections for vacuum polarization and electron self-energy [32,36]. The eigenvalues and eigenvectors of this perturbed matrix give the energies and atomic wave functions used to cal-

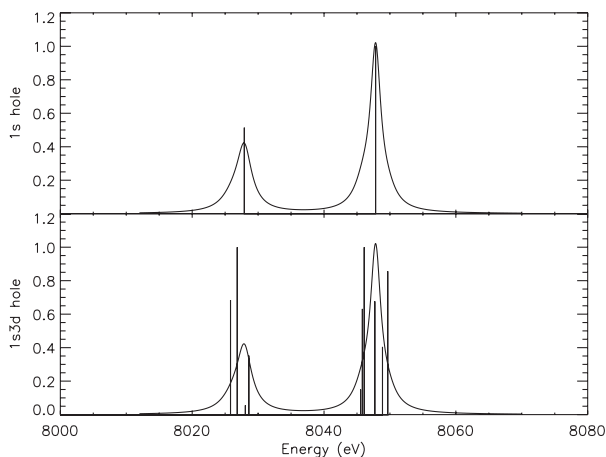


FIG. 2. Calculated energies and relative intensities resulting from diagram and satellite transitions for Copper  $K\alpha$ , overlaid with the experimental spectrum and normalized.

TABLE I. Convergence of  $K\alpha$  diagram energies. The two experimental values are as-reported for the full spectrum calibration [8] or reconstructed (Table II), including the satellite spectrum, which is nontrivial to deconvolve. However, expected diagram energies would be approximately 0.01 eV higher than the full spectrum for  $K\alpha_1$  and perhaps a few 0.01 eVs for  $K\alpha_2$  (see text).

CSFs	Excitations	Orbitals	$2p_{1/2} \rightarrow 1s$ (eV)	$2p_{3/2} \rightarrow 1s$ (eV)
3	0	...	8030.79	8050.82
53	1	$4d$	8028.85	8048.67
203	1	$4p4d4f$	8026.92	8046.87
20897	2	$4p4d4f$	8027.91	8047.84
Reconstructed [8]			8027.88(0.13)	8047.84(0.06)
Full Spectrum [8]			8027.85(0.01)	8047.83(0.01)

TABLE II. Convergence of  $K\alpha$  diagram transition strengths for length and velocity gauges. These converge to 0.05%.

CSFs	Excitations	Orbitals	$A^L$ ( $10^{14} \text{ s}^{-1}$ )	$A^V$ ( $10^{14} \text{ s}^{-1}$ )	$A^L/A^V$
$2p_{1/2} \rightarrow 1s$					
3	0	$\dots$	2.07250	2.08825	0.9926
53	1	$4d$	2.03613	2.05011	1.1518
203	1	$4p4d4f$	2.05644	2.06283	0.9969
20897	2	$4p4d4f$	2.04922	2.04854	1.0003
$2p_{3/2} \rightarrow 1s$					
3	0	$\dots$	1.02343	1.03100	0.9926
53	1	$4d$	1.00653	1.01317	0.9934
203	1	$4p4d4f$	1.00574	1.00929	0.9965
20897	2	$4d4p4f$	1.00580	1.00544	1.0004

culate transition probabilities. The improved agreement of the oscillator strengths in the length and velocity gauges  $A^L$  and  $A^V$  as the CSF set is enlarged (Table II) strongly endorses the quality of the ASF representations. The difference in transition strengths between the two gauges remains one of the few methods [31,37] for demonstrating convergence without reference to experiment. Although this is already the most elaborate calculation yet published for the Cu  $K\alpha$  lines, we are continuing to investigate the effect of adding further configurational states to ensure that important correlation effects have not been omitted.

Deutsch *et al.* fitted their experimental spectrum with a sum of Lorentzians, including offsets for energy nonconvergence. The line strengths were calculated using orbitals from the initial state: Deutsch *et al.* did not have biorthogonal software so performed configuration interaction calculations with frozen orbitals to calculate oscillator strengths. The difference between  $A^L$  and  $A^V$  was within about 10% for all and 5% for the strongest line. Table II shows that our theoretical strengths for diagram lines agree to <1% for the simplest calculation, improving to <0.04% in the most elaborate calculation. Our predicted energies and relative intensities of the diagram lines are shown in Fig. 2.

The lower part of Fig. 2 shows our predictions for satellite lines. Our procedure differs from that of Deutsch *et al.* as we include the weakly bound  $4s$  electron. In their calculation, the two lower atomic states,  $2p_{1/2}$  and  $2p_{3/2}$  were obtained using different energy functionals, which repressed potentially crucial mixing of the inner orbitals. We therefore retained the  $4s$  electron, and calculated the  $J = 1$  states, so we could use the same orbital basis for the common upper state as well as both lower states. This assumption gives a good description of the  $1s$  hole state for other values of  $J$ . A spectator  $3d$  hole breaks the symmetry of the single hole configuration, giving structure to the  $K\alpha$  spectrum. The number of CSFs needed to describe these states increases greatly so that convergence with enlargement of the CSF set is more difficult to achieve. The most effective procedure appears to start

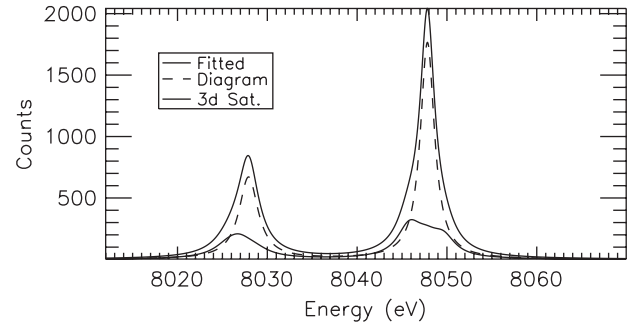


FIG. 3. Theory and experiment for Copper  $K\alpha$ . The fitted line and contributions from both the  $1s$  and  $1s3d$  initial states are shown together. The experimental curve and error bars are indistinguishable.

with the lowest state of each set of split diagram lines and to add CSFs progressively with single and double excitations from the  $n = 3$  to  $n = 4$  subshells. This gave oscillator strengths whose gauge differences were within about 1%. We then performed more modest MCDHF calculations for each  $J\pi$  symmetry to get a representation of the whole spectrum. This enabled us to avoid difficulties of false convergences among the closely split levels.

Figure 2 shows that the [ $3d$ ] hole states make the  $2p_{3/2}$  orbital more diffuse so that its overlap with  $1s$  is less than that of the  $2p_{1/2}$  orbital. The experimental spectrum can now be fitted with just three parameters: the widths of  $K\alpha_1$  and  $K\alpha_2$  lines and a Gaussian difference width  $w_d$  between the widths of the diagram and satellite lines (satellite lines will be broader than diagram lines). The resulting level of accuracy is not surpassed in the literature to our knowledge.

Figure 3 shows the fitted spectrum, with contributions from both  $1s$  and  $1s3d$  initial states, with residuals in Fig. 4. The  $\chi_r^2$  of the fit using only diagram lines gave  $\chi_r^2 = 2.65$  while inclusion of satellites dropped this to 0.46. Using the relative populations  $p_d$  and  $p_s$  of the diagram and satellite lines yields a total integrated intensity ratio  $I(K\alpha_1)/I(K\alpha_2) = 0.522 \pm 0.003$ . The ratio has been reported as low as  $0.507 \pm 0.014$  [11], while the most reliable determination is  $0.518 \pm 0.021$  [8], both consistent with our result. Theoretical and derived (experimental) component widths are presented in Table III. While total spectral widths vary widely depending upon the resolution, authors have attempted to derive raw widths by removing

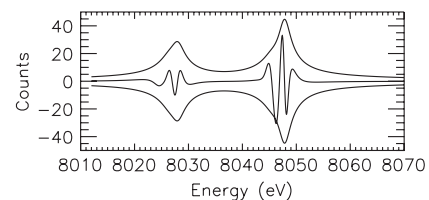


FIG. 4. Residual between experiment and theory. The two curves bounding the residue denote  $\pm\sigma$  from experiment.

TABLE III. Parameters and standard deviations for  $K\alpha$ . Standard deviations in brackets are in the last significant figures.

Parameter	Widths (s.d.) eV				
	Present	[17]	[19]	literature	
Component					
$2p_{3/2}$	2.55(11)	2.68	1.81(5)	2.07 [38]	2.14 [39]
$2p_{1/2}$	1.87(10)	2.08	2.93(7)	2.96 [38]	2.15 [39]
$2p_{3/2}3d$	3.86(24)	2.75	1.21(15)	...	...
$2p_{1/2}3d$	3.18(25)	2.75	1.09(15)	...	...
% Populations					
Diagram	71.0(25)	69	72(3)		
Satellite	29.0(25)	31	28(3)	5.5 [40]	13 [41]

instrumental broadening. Results vary from 2.28 eV to 2.47 eV for  $K\alpha_1$  and from 2.78 eV to 3.49 eV for  $K\alpha_2$ . A few authors have attempted to fit diagram or satellite subcomponent widths as in Table III with similar results. This is a limitation of the current and previous approaches, in that the subcomponent widths are fitted and there is little constraint from good theory. Whilst excellent results have been obtained, there is clearly room for improvement of experiment and theory.

The summed spectral profile is well accounted for by the presence of the spectator lines. The relatively large variation in the fitted satellite contributions from Table III is due to correlation of the fitting approaches with noise in the experimental data. The residual in Fig. 4 is well bounded by the statistical error. The theoretical understanding of shake processes is still developing. Estimations for satellite and diagram cross sections vary greatly [14,40,41] and the agreement with experiment (Table III) is relatively poor. This suggests the need to investigate these effects across a broad range of atomic systems. Comparisons with other similar elements can provide insight into the magnitude and nature of these poorly understood processes.

We have shown that the ratio of  $K\alpha$  line intensities can be explained by considering the atomic wave function in detail. Using biorthogonal CSF sets, we have investigated a difficult problem involving near degenerate eigenstates, slowly converging sets of levels, and calculated the diagram line profiles of copper to within 0.05% of their experimental value, with even better convergence on their energies. We have produced an *ab initio* derivation of the intensities and energies of diagram and spectator lines for copper that were able to account, to a high degree of accuracy, for the full  $K\alpha$  spectrum (Fig. 3). In particular, our determination of the ratio for  $I(K\alpha_2)/I(K\alpha_21)$ ,  $0.522 \pm 0.003$ , is in agreement with experiment. This gives confidence in the quality of the theoretical model and the care taken for the corresponding experiments.

\*chantler@unimelb.edu.au

[1] N. Bohr, Philos. Mag. **25**, 10 (1913).

- [2] M. Niering *et al.*, Phys. Rev. Lett. **84**, 5496 (2000).  
 [3] R. Penrose, *The Emperor's New Mind* (OUP, Oxford, 1989).  
 [4] C. T. Chantler, Radiat. Phys. Chem. **71**, 611 (2004).  
 [5] C. T. Chantler *et al.*, Phys. Rev. A **73**, 012508 (2006).  
 [6] C. T. Chantler *et al.*, Phys. Rev. A **62**, 042501 (2000).  
 [7] C. T. Chantler *et al.*, Phys. Rev. A **76**, 042116 (2007).  
 [8] G. Hölzer *et al.*, Phys. Rev. A **56**, 4554 (1997).  
 [9] J. H. Williams, Phys. Rev. **44**, 146 (1933).  
 [10] J. H. McCrary *et al.*, Phys. Rev. A **4**, 1745 (1971).  
 [11] S. I. Salem and R. J. Wimmer, Phys. Rev. A **2**, 1121 (1970).  
 [12] P. L. Lee and S. I. Salem, Phys. Rev. A **10**, 2027 (1974).  
 [13] L. G. Parratt, Phys. Rev. **50**, 1 (1936).  
 [14] J. H. Scofield, Phys. Rev. A **9**, 1041 (1974).  
 [15] W. J. Kuhn and B. L. Scott, Phys. Rev. A **34**, 1125 (1986).  
 [16] C. Froese-Fischer, Comput. Phys. Commun. **4**, 107 (1972).  
 [17] M. Deutsch *et al.*, Phys. Rev. A **51**, 283 (1995).  
 [18] J. W. Cooper, Phys. Rev. A **38**, 3417 (1988).  
 [19] W. C. Sauder, J. R. Huddle, J. D. Wilson, and R. E. Lavilla, Phys. Lett. A **63**, 313 (1977).  
 [20] R. E. LaVilla, Phys. Rev. A **19**, 717 (1979).  
 [21] N. Maskil and M. Deutsch, Phys. Rev. A **37**, 2947 (1988).  
 [22] M. Deutsch and M. Hart, Phys. Rev. B **26**, 5558 (1982).  
 [23] S. Doniach and M. Sunjic, J. Phys. C **3**, 285 (1970).  
 [24] J. Finster, G. Leonhardt, and A. Meisel, J. Phys. (Paris), Colloq. **32**, (1971).  
 [25] K. Tsutsumi and H. Nakamori, *X-ray Spectra and Chemical Binding* (Fotodruck Frank OHG, Munchen, 1973).  
 [26] I. P. Grant, Proc. R. Soc. A **262**, 555 (1961).  
 [27] I. P. Grant, J. Phys. B **19**, 3187 (1986).  
 [28] I. P. Grant, B. J. McKenzie, P. H. Norrington, D. F. Mayers, and N. C. Pyper, Comput. Phys. Commun. **21**, 207 (1980).  
 [29] R. Couch and B. L. Scott, Phys. Rev. A **44**, 3016 (1991).  
 [30] M. Deutsch, E. Forster, G. Holzer, J. Hartwig, K. Hamalainen, C. C. Kao, S. Huotari, and R. Diamant, J. Res. Natl. Inst. Stand. Technol. **109**, 75 (2004).  
 [31] C. Froese Fischer, T. Brage, and P. Jonsson, *Computational Atomic Structure: An MCHF Approach* (CRC Press, New York, 1997).  
 [32] I. P. Grant, *Relativistic Quantum Theory of Atoms and Molecules: Theory and Computation* (Springer, New York, 2007).  
 [33] J. Olsen, M. R. Godefroid, P. Jönsson, P. A. Malmqvist, and C. F. Fischer, Phys. Rev. E **52**, 4499 (1995).  
 [34] P. Jönsson and C. F. Fischer, Phys. Rev. A **57**, 4967 (1998).  
 [35] P. Jönsson, X. He, C. Froese Fischer, and I. P. Grant, Comput. Phys. Commun. **177**, 597 (2007).  
 [36] I. P. Grant, *Springer Handbook of Atomic, Molecular and Atomic Physics* (AIP, New York, 1996), Chap. 22.  
 [37] C. Froese-Fischer, *The Hartree-Fock Method for Atoms* (Wiley, New York, 1977).  
 [38] L. I. Yin, I. Adler, M. H. Chen, and B. Crasemann, Phys. Rev. A **7**, 897 (1973).  
 [39] M. H. Chen, B. Crasemann, and H. Mark, Phys. Rev. A **24**, 177 (1981).  
 [40] A. G. Kochur and V. A. Popov, Radiat. Phys. Chem. **75**, 1525 (2006).  
 [41] Y. Ito, T. Tochio, H. Oohashi, and A. M. Vlaicu, Radiat. Phys. Chem. **75**, 1534 (2006).